Journal of Materials Chemistry C

ROYAL SOCIETY OF CHEMISTRY

PAPER

View Article Online
View Journal | View Issue

Cite this: J. Mater. Chem. C, 2021, 9, 5167

Remarkable smectic phase behaviour in odd-membered liquid crystal dimers: the CT6O.*m* series†

Rebecca Walker, *[a] Damian Pociecha, [b] John M. D. Storey, [a] Ewa Gorecka [b] and Corrie T. Imrie [a]

Received 24th February 2021,
Accepted 24th March 2021

DOI: 10.1039/d1tc00904d

rsc.li/materials-c

The syntheses and characterisation of the first ten homologues of the (3^4-[6-(4-{(*E*)-[(4-alkylphenyl)imino]methyl}phenoxy)-hexyl][1^1,2^1:2^4,3^1-terphenyl]-1^4-carbonitriles (CT6O.*m*) are reported. Below the conventional nematic phase, N, a rich smectic polymorphism is observed. CT6O.*m* homologues with m = 1–9 show a series of up to four smectic phases, namely: an intercalated biaxial smectic A_b phase, a modulated phase made of tilted biaxial SmC layer fragments, a non-tilted biaxial hexatic-type phase termed the SmX phase, and a soft crystalline lamellar phase, SmY. The longest homologue, CT6O.10, exhibits a different sequence of smectic phases below the N phase: an uniaxial SmA phase, a biaxial SmA_b phase, a tilted SmC phase, and the soft crystalline SmY phase. The assignment of these phases was confirmed using a combination of polarised optical microscopy, X-ray diffraction and optical birefringence studies. In CT6O.10 only the SmC has an intercalated structure of molecules; while the smectic phases either side show interdigitated molecular packing arrangement. The strong biaxiality of the SmC phase results in an unusual switching mode detected under the application of an electric field, in which by coupling the dielectric anisotropy with the electric field, molecules in cells with planar anchoring reorient to give an optical texture without tilt domains, and the switching is accompanied by a considerable increase in the measured birefringence.

Introduction

The experimental discovery of the twist-bend nematic phase, N_{TB}, some 35 years after it was first proposed by Meyer,[1] and later independently by Dozov,[2] has stimulated intense research interest into the structure–property relationships of odd-membered liquid crystal dimers.[3] In the N_{TB} phase the molecules arrange in a heliconical superstructure of nanoscale periodicity, while retaining a random distribution of their centres of mass. Unlike the cholesteric, (chiral nematic, N*) phase, for which the director twists around an axis perpendicular to the long axes of the molecules, the director in the N_{TB} phase is tilted at an arbitrary angle $\theta < 90^\circ$ with respect to the helix axis and precesses on a cone, forming an oblique helix of pitch about two orders of magnitude shorter than that found in the N* phase, and equal to just 2–3 molecular lengths.[4–6] The N_{TB} phase can be considered as a generalised case of the N* phase and has been described as the 'structural link' between the N and N* phases. Undoubtedly the most fascinating feature of this phase is that its chiral superstructure is formed despite the constituent molecules being chemically achiral, and indeed the N_{TB} phase represents the first example of such spontaneous chiral symmetry breaking in a fluid system with no spatial ordering. As this induction of chirality is spontaneous, there is an equal probability of formation of either handedness of helix and hence the N_{TB} phase comprises of doubly degenerate locally chiral domains of opposite handedness, giving a conglomerate-type chiral phase. The presence of molecular chirality removes this degeneracy and the chiral N_{TB} phase is observed.[7] It is widely believed that the key structural requirement for the observation of the N_{TB} phase is a bent molecular shape, and indeed theory predicts that the N_{TB} phase is formed for just a narrow range of molecular curvatures.[8] In his seminal work, Dozov also used symmetry arguments to predict the existence of heliconical smectic phases.[2] The majority of N_{TB} phases either crystallise or vitrify upon cooling, however more recently N_{TB}–smectic transitions have been observed.[9–15]

Recently, we reported two examples of an N_{TB}–heliconical smectic phase transition in bent achiral liquid crystal dimers and termed this lamellar phase SmC_{TB}.[16–18] A helical smectic

[a] Department of Chemistry, School of Natural and Computing Sciences, University of Aberdeen, AB24 3UE Scotland, UK. E-mail: rebecca.walker@abdn.ac.uk
[b] University of Warsaw, Faculty of Chemistry, ul. Zwirki i Wigury 101 02-089 Warsaw, Poland

† Electronic supplementary information (ESI) available: Synthetic procedures and analytical data; supporting figures. See DOI: 10.1039/d1tc00904d

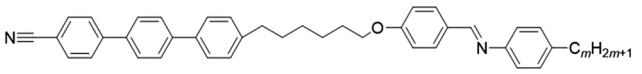

Fig. 1 Structure of the 3^4-[6-(4-{(*E*)-[(4-alkylphenyl)imino]methyl}-phenoxy)-hexyl][1^1,2^1:2^4,3^1-terphenyl]-1^4-carbonitrile series (CT6O.*m*, where m = 1–10).

phase formed by achiral molecules has been suggested also for a rigid bent core liquid crystal.[19] It appears, however, that a number of 'SmC_{TB}' phases with differing 'clock-like' molecular arrangements are possible, similar to the SmC* subphases observed for chiral molecules.[20] In one set of these materials a hexatic-type phase was also observed in which the chirality is expressed on two length scales, nanoscale helices and mesoscopic helical filaments.[16] We are still at an early stage in establishing and understanding how the bent molecules pack into smectic phases and the properties such phases exhibit.

Here, we present a series of new liquid crystal dimers, analogues of the previously reported CB6O.*m* series, the m = 10 homologue of which was the first reported to exhibit an N_{TB}–SmC_{TB} phase transition.[17,18] We extend the cyanobiphenyl mesogenic unit to a cyanoterphenyl moiety to give the CT6O.*m* series, (3^4-[6-(4-{(*E*)-[(4-alkylphenyl)imino]methyl}phenoxy)-hexyl][1^1,2^1:2^4, 3^1-terphenyl]-1^4-carbonitriles), see Fig. 1. Inserting a third *para*-linked phenyl ring into a biphenyl mesogenic core greatly enhances the molecular shape anisotropy and polarisability of the unit, the main features which promote liquid crystallinity in rod-like molecules. Thus, terphenyl-based molecules exhibit higher transition temperatures than their biphenyl-based counterparts. The cyanobiphenyl moiety features in some of the most studied twist-bend nematogenic dimers, see for example,[21,22] whereas the terphenyl moiety has only rarely been included in reports focussed on structure–property relationships of the N_{TB} phase, see for example,[10,23–25] many of which were found to exhibit twist-bend nematic phases below a conventional nematic phase. The CT6O.*m* series was designed in the expectation that the mixed core interactions would be enhanced, which may in turn stabilise smectic phases and reveal new examples of the SmC_{TB} phase.

Experimental

Synthesis

The synthesis of the CT6O.*m* series followed the route outlined in Scheme 1. The route to (2) is identical to that reported earlier for the synthesis of CB6O.*m*.[18] A Suzuki–Miyaura reaction coupled 4-(6-bromohexyl)-4′-bromo-1,1′-biphenyl (2) to cyanoboronic acid to give the terphenyl-based compound (3), which underwent a Williamson ether synthesis with hydroxybenzaldehyde to yield (4). This was subsequently combined with the relevant aniline to form the desired Schiff's base (5). Detailed syntheses and analytical data for all intermediates and final products are given in the ESI.†

Characterisation

Thermal measurements. The phase behaviour of the dimers was studied by differential scanning calorimetry using a Mettler-Toledo DSC820 fitted with an intracooler and calibrated using indium and zinc as standards. Heating and cooling rates were 10 °C min^{-1} and all samples were measured under a nitrogen atmosphere. Transition temperatures and associated enthalpy changes were extracted from the second heating trace unless otherwise noted. For each sample, two aliquots were measured and the data listed are the average of the two sets of data.

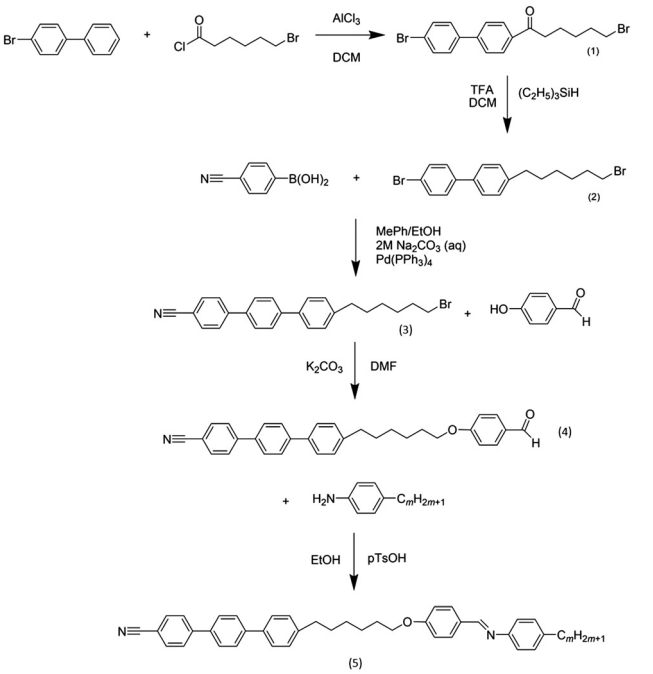

Scheme 1 Synthetic route to the CT6O.*m* series.

Optical studies. For phase characterisation polarised light microscopy was performed using an Imager A2m polarizing microscope equipped with a Linkam heating stage. Birefringence was measured in 3 micron thick glass cells with planar anchoring using a setup made of photoelestic modulator (PEM-90, Hinds) a halogen light source (Hamamatsu LC8) equipped with a narrow band pass filter (532 nm), a photodiode (FLC Electronics PIN-20) and a lock-in amplifier (EG&G 7265).

Electrooptic and dielectric studies. Electrooptic and dielectric studies were performed in 3 micron thick glass cells having transparent ITO electrodes covered with surfactant for planar anchoring. Dielectric permittivity as a function of frequency and temperature was measured with an Impedance Analyzer Solarton SI1260. Electric field was applied to the cells using function generator SRS DS345 equipped with FLC A400 voltage amplifier.

X-Ray diffraction. The small angle X-ray diffraction (SAXRD) patterns for powder samples were obtained with a Bruker Nanostar system using CuKα radiation and patterns were collected with an area detector VANTEC2000. The temperature of the sample was controlled with precision of ±0.1 K. Broad angle diffractograms (WAXS) were obtained with a Bruker D8 Discover system (CuKα line, Goebel mirror, point beam collimator, VANTEC-1 linear detector). Samples were prepared as droplets on a heated surface.

Results and discussion

The transition temperatures and associated entropy changes for the CT6O.*m* series are summarised in Table 1, and the dependence of the temperatures on *m* is shown in Fig. 2. As a consequence of the introduction of the third phenyl ring, the clearing temperatures of the CT6O.*m* series are over 100 K higher than those of the biphenyl counterparts, the CB6O.*m* series (Fig. S1, ESI†).[18] All ten homologues are enantiotropic nematogens. The nematic phase was assigned using polarised optical microscopy (POM): between untreated glass slides, a characteristic schlieren texture containing two- and four-brush point defects, which flashed under application of mechanical stress, was observed, and uniform alignment was seen in cells with planar anchoring (HG cells), shown in Fig. 3. The low values of the associated entropy change, ΔS_{NI}, are consistent with the nematic phase assignment (Table 1).

A twist-bend nematic phase is not observed on cooling the N phase for any length of alkyl terminal chain, *m*, but instead a sequence of up to four smectic phases is found. The smectic phases have been characterised using a combination of optical methods and X-ray diffraction.

The highest temperature smectic phase for homologues *m* = 1–9, has been assigned as an intercalated biaxial smectic A phase (SmA_b). The SmA_b phase is an orthogonal lamellar phase in which molecular rotation around the long axis is restricted. The restricted rotation results in different 'in-plane' polarizabilities, higher for the light polarized in the direction containing the dimer planes and lower perpendicular to this plane (Fig. S2, ESI†). The different polarizabilities translate to different in-layer refractive indices and therefore the SmA_b phase exhibits optical biaxiality, which manifests as optical anisotropy when observed along the layer normal with POM. The schlieren texture (in cells with homeotropic anchoring, HT) contains predominantly two-brush point defects (Fig. 3). In HG cells, when viewed between crossed polarisers the light extinction directions are along the polariser and analyser, and the careful examination of the texture reveals regions of slightly different birefringence. The regions with lower birefringence dominate showing that most molecules are oriented with their dimer planes parallel the glass substrate. In wedge cells with HT anchoring, a characteristic texture was found, with stripes of different birefringence running across the schlieren pattern

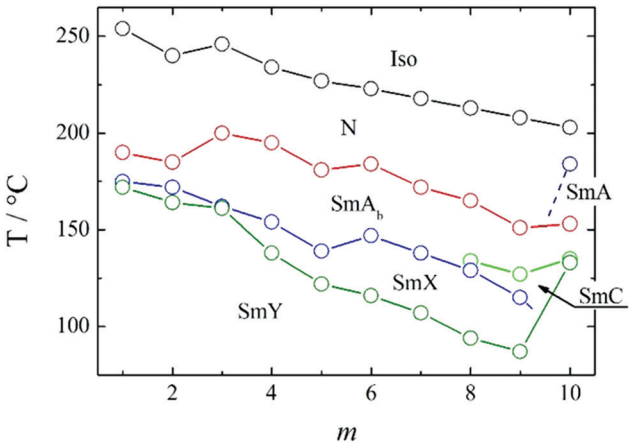

Fig. 2 Phase diagram for the homologous series, CT6O.*m*. Melting points have been omitted for clarity.

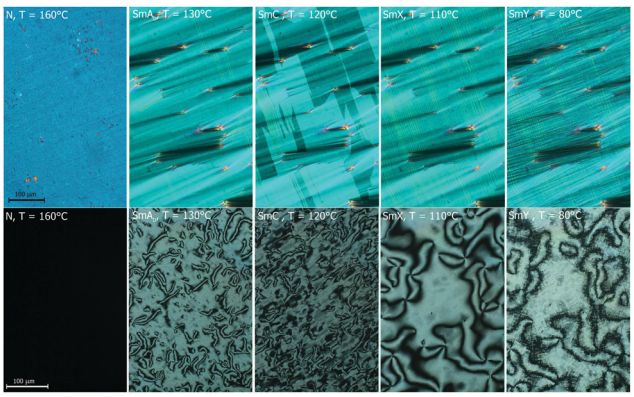

Fig. 3 Representative optical textures for LC phases exhibited by CT6O.9 homologue in a sample with planar (upper row) and homeotropic (lower row) anchoring. In each row the same area of the sample is presented.

(Fig. S3, ESI†).[26] For CT6O.*m* homologues with *m* = 1–9, the lowest angle signal in the X-ray diffraction pattern of the SmA_b phase corresponds to ~17–21 Å – approximately half the molecular length, *l*, indicating a locally intercalated structure (Fig. 4). The broad high-angle diffraction signal is indicative of liquid-like ordering within the layers.

Table 1 Phase transition temperatures and associated entropy changes (in parentheses, scaled by R) for the CT6O.*m* series

m	M.p.	SmY		SmX		SmC		SmA_b		SmA		N		Iso
1	179 (4.66)	●	172 (3.06[a])	●	175[a]			●	190 (2.08)			●	254 (0.25)	●
2	173 (5.11)	●	164 (2.27[a])	●	172[a]			●	185 (1.54)			●	240 (0.31)	●
3	164 (3.05)	●	161 (2.95[a])	●	162[a]			●	200 (2.04)			●	246 (0.36)	●
4	148 (5.12)	●	138 (1.35)	●	154 (0.87)			●	195 (2.10)			●	234 (0.38)	●
5	132 (4.07)	●	122 (0.92)	●	139 (0.70)			●	181 (1.58)			●	227 (0.32)	●
6	121 (1.85)	●	116 (0.79)	●	147 (0.86)			●	184 (1.59)			●	223 (0.33)	●
7	128 (3.27)	●	107 (0.53)	●	138 (1.05)			●	172 (2.01)			●	218 (0.39)	●
8	132 (5.71)	●	94 (0.36)	●	129 (0.22)	●	134 (0.30)	●	165 (1.94)			●	213 (0.31)	●
9	146 (8.85)	●	87 (0.40)	●	115 (0.34)	●	127 (0.42)	●	151 (1.67)			●	208 (0.27)	●
10	109 (14.73)	●	133 (4.68[a])			●	135[a]	●	153 (0.08)	●	184 (0.06)	●	203 (0.31)	●

[a] $\Delta S/R$ is a combined value of those associated with both phases due to peak overlap in the DSC trace.

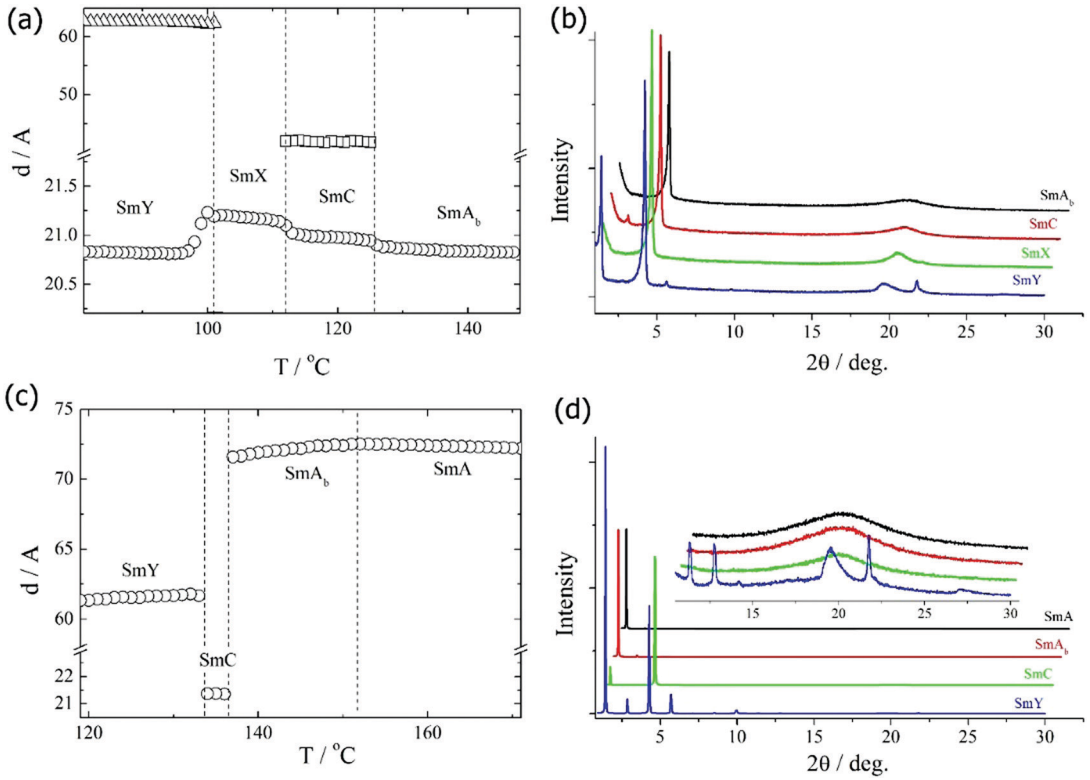

Fig. 4 Temperature evolution of distances related to low angle signals in the XRD patterns for homologues (a) CT6O.9 and (c) CT6O.10. In the SmA_b and SmX phases of CT6O.9, the structure is simple lamellar while the SmC and SmY are modulated phases, as evidenced by the presence of additional low-angle signals. In (b) and (d) broad angle diffractograms for CT6O.9 and CT6O.10, respectively, showing evolution of the in-plane order in consecutive smectic phases.

The phase shown by homologues with m = 8 and 9 directly below the SmA_b phase is a tilted smectic phase with a synclinic arrangement of the molecules in consecutive layers. The synclinically tilted structure is evidenced by the appearance of alternating domains across the focal conic optical texture with different extinction directions (Fig. 3); each domain can be brought into extinction condition upon rotation of the sample (Fig. S4, ESI†), allowing for the determination of the tilt angle, $\theta \sim 5$ deg.

The phase, when examined by dielectric spectroscopy appears to be non-polar (no dielectric relaxation mode was visible in the range up to MHz, Fig. S5, ESI†). However, on application of an electric field, a clear optical response has been observed, the tilted domains disappear and the extinction direction becomes along the layer normal (Fig. 5), while the birefringence increases (inset in Fig. 6). The switching is distinctly different than observed for bent-core mesogens in SmCP type phases; in the ferroelectric SmC_SP_F phase under an electric field, domains interchange the extinction directions without a change of birefringence, while in the antiferroelectric $SmCsP_A$ phase the synclinic domains disappear upon inducing an anticlinic ferro-structure but this is accompanied by a significant decrease of birefringence. The switching observed for the materials studied here may be explained in terms of a dielectrically induced rotation of the molecules on the tilt cone, as observed experimentally such rotation is not accompanied by repolarization current. Apparently at the transition from the SmA_b to the SmC phase, molecules tilt with respect to the layer normal in such a way that their dimer planes are parallel to the tilt plane defined by director and layer normal (Fig. 5). On application of an electric field in HG cells the molecules rotate, keeping the orientation of their dimer planes unchanged with respect to the tilt plane (Fig. 5), and as a result the birefringence increases while the average projection of the long molecular axis on the cell substrate plane adopts the rubbing direction. The tilted domains of lower birefringence are restored when the electric field is removed. Apparently, this new type of switching is possible because of strong coupling between the tilt and orientation of the molecular plane, which prevents the rotation of molecules along their long axis without changing the tilt direction. In the XRD patterns of the SmC phase, the most intense small-angle signal corresponds to half the molecular length (Fig. 4), as in the SmA_b phase, although a second, weak and slightly incommensurate signal is also present at a position corresponding to almost the full molecular length ($\sim$40 Å). This implies frustration in the structure, with competition between intercalated and monolayer packing arrangements. As a result of the frustration the SmC phase has a modulated structure constructed from biaxial SmC layer fragments of length $\sim$250 Å.[27] The broad wide-angle X-ray diffraction signal, only slightly narrower that in the preceding SmA_b phase, indicates the lack of long range in-plane order

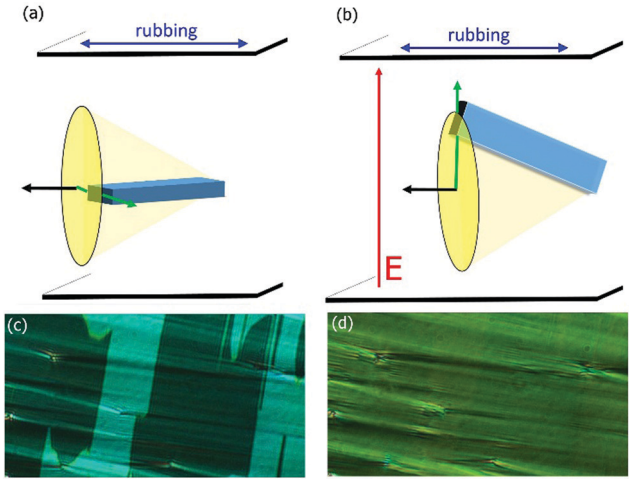

Fig. 5 (a) In the SmC phase molecules tilt with respect to the layer normal (black arrow) in such a way that the dimer plane is parallel to the tilt plane (defined by the layer normal and the tilt direction – green arrow). Thus, if observed in cells with planar anchoring (bookshelf geometry), the extinction direction is inclined from the layer normal (rubbing direction). Due to double degeneration of tilt direction two kinds of domains are observed (c), which can be brought into extinction conditions upon rotation of the cell with respect to crossed polarizers. (b) Under application of electric field E molecules rotate on a tilt cone due to dielectric susceptibility anisotropy in such a way that the dimer plane remains parallel to the tilt plane, thus the extinction direction (defined by the projection of long molecular axis on the cell surface) aligns along the rubbing direction. The switching therefore causes the disappearance of tilt domains as well as an increase of measured birefringence (d).

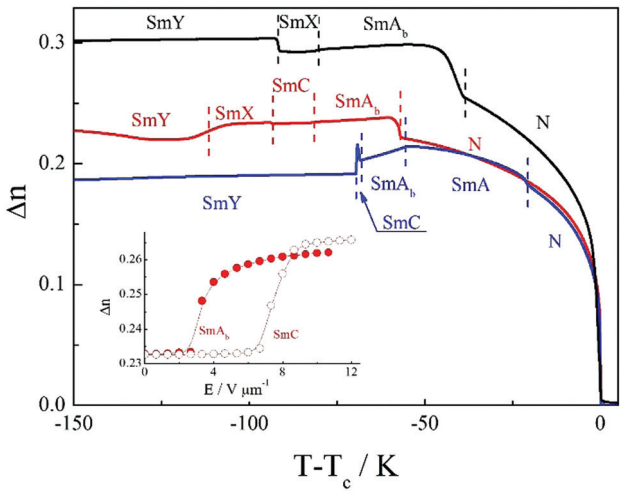

Fig. 6 Optical birefringence for CT6O.m dimers with m = 4 (black line), m = 9 (red line) and m = 10 (blue line) measured in cells with planar anchoring. In the inset the increase of optical birefringence under an applied electric field, E, measured in the SmA_b and SmC phases of CT6O.9.

(Fig. 4). Unfortunately, a sufficiently well-aligned sample could not be obtained in the modulated SmC phase to establish whether the plane of modulation is parallel or perpendicular to the tilt plane.

The additional smectic phases on the phase diagram (Fig. 2), denoted as SmX and SmY have more ordered structures as indicated by a narrowing of the high angle signals in their X-ray diffraction patterns (Fig. 4). In the SmX phase a single high angle signal is detected suggesting that the phase is a hexatic-type (possibly biaxial SmB_{hex} phase), whereas in the SmY phase the signal splits into several, indicating long range positional ordering of the molecules inside the layer (a crystalline-type smectic phase, possibly SmE phase[12]). In both, SmX and SmY phases the most intense low angle diffraction signal also corresponds to half the molecular length, only a small increase in the layer spacing is seen at the SmA_b–SmX or SmC–SmX phase transitions. In the SmY phase the layer spacing decreases and the presence of an additional signal at a lower diffraction angle suggests the phase has a modulated structure, with an additional in-plane density wave.[28–30] Upon transition from the SmC phase to the SmX phase, the tilted domains disappear, and the phase returns to an optical texture with extinction directions along the polarizer and analyser with the optical birefringence nearly unchanged (Fig. 3). In cells with planar anchoring the SmY phase also exhibits a focal conic fan-like pattern, only differing from that seen for the SmA_b and SmX phases by a small change in birefringence at the transition (Fig. 6). In cells with HT anchoring a plate-like mosaic texture is seen in the SmY phase (Fig. 3).

The longest homologue, the decyl-terminated CT6O.10, behaves quite differently. Specifically, it shows a sequence of four smectic phases below the nematic phase, and the highest temperature smectic phase appears at a considerably higher temperature than for the preceding homologue. Moreover, this phase gives a homeotropic texture in HT cells, indicative of a uniaxial smectic A phase. On cooling, the homeotropic texture is replaced by weakly birefringent schlieren, while in wedge cells stripe domains appear confirming formation of the SmA_b phase. Interestingly, the X-ray diffraction experiments revealed that both the SmA and SmA_b phases have a layer spacing of approximately 72 Å, corresponding to 1.7 times the molecular length of CT6O.10 ($l \approx 43$ Å) (Fig. 4). This strongly suggests an interdigitated bilayer arrangement of the molecules in these lamellar phases, with segregation of the cyano groups at every second layer interface. The diffuse wide-angle diffraction signal indicates liquid-like ordering within the smectic layers. Although the layer spacing in the SmA_b phase seen for CT6O.10 is dramatically different to that in the shorter homologues, the temperature of the phase appearance on cooling follows the general trend in the phase diagram (Fig. 2). Below the SmA_b phase, a short range smectic C phase is observed, indicated by a fan texture with tilted domains in HG cells and a bright schlieren texture in HT cells. Surprisingly, the most intense low angle XRD signal in the SmC phase corresponds to half the molecular length (Fig. 4), suggesting that this phase has the intercalated structure, similar to that observed for the shorter homologues. The SmC phase retains the liquid-like in-plane ordering present in the higher temperature SmA and SmA_b phases. The lowest temperature smectic phase exhibited by CT6O.10, the SmY phase, appears optically as a platelet- or mosaic-like texture, and has an X-ray diffraction pattern with the lowest angle signal located at approximately

1.5 times the molecular length l, indicating a shift back to an interdigitated molecular arrangement, similar to those seen for the SmA and SmA_b phases. There are more than 10 harmonics related to the layer periodicity observed in the XRD pattern of the SmY phase, suggesting that this is a highly ordered lamellar phase, presumably a soft-crystal type lamellar phase. The signals in the wide angle region are considerably narrower than those seen in the preceding phases, and have a very similar pattern to those seen in the SmY phase of the shorter homologues.

The formation of intercalated smectic phases in cyanobiphenyl-based nonsymmetric dimers, and higher oligomers, is driven by a specific favourable interaction between the unlike mesogenic units.[31–33] In the intercalated structure, the spacers and terminal chains are mixed. If the mesogenic units are approximately the same size, then, if the terminal chain length exceeds that of the spacer, the intercalated arrangement is destabilised, and smectic behaviour tends to be extinguished. On further increasing the terminal chain length, interdigitated smectic phases are observed stabilised by the interaction between the polar and polarisable cyanobiphenyl groups. In this arrangement the spacers and terminal form separation regions. In the CT6O.*m* series, however, the mismatch in the lengths of the mesogenic units allows for terminal chain lengths greater than the spacer length to be accommodated and an intercalated smectic A phase is observed for CT6O.9. To our knowledge CT6O.10 is the first example of a single compound in which a transition between intercalated and interdigitated phases is seen and the driving force for this remarkable behaviour is unclear.

Conclusions

In summary, we have synthesised a new series of odd-membered non-symmetric liquid crystalline dimers, the CT6O.*m* series, and characterised their phase behaviour using a combination of optical and X-ray diffraction techniques. Comparing the CT6O.*m* dimers to the previously reported CB6O.*m* dimers[18] it is clear that replacing a biphenyl unit by a terphenyl one has a dramatic effect on the stability of liquid crystalline phases. In both series, the highest temperature phase is the conventional nematic phase, however the clearing temperatures, T_{NI}, are by some 100 K higher for the terphenyl compounds (Fig. S1, ESI†). This is a result of the greater shape anisotropy of the mesogenic unit and significantly enhanced intermolecular interactions. Furthermore, a clear odd–even effect seen in T_{NI} on varying m is evident in the CB6O.*m* series, whereas it quickly attenuates for the CT6O.*m* series. The absence of the odd–even effect in the terphenyl-based series may be attributed to the dominant effect of increasing terminal chain length being the dilution of the interactions between the larger mesogenic units on increasing the volume fraction of the alkyl chains. The twist-bend nematic phase observed for all the members of the CB6O.*m* series is not seen in their terphenyl analogues. Instead, a rich smectic polymorphism is observed, apparently the additional phenyl ring in one of the mesogenic cores stabilises smectic behaviour to such a large extent that it precludes the observation of the twist-bend nematic phase. For the CT6O.*m* homologues with m = 1–9, a series of up to four smectic phases is observed on cooling from the N phase, namely: an intercalated biaxial smectic A_b phase, a modulated phase made of tilted biaxial SmC layer fragments, a non-tilted biaxial hexatic-type phase termed the SmX phase, and a soft crystalline lamellar phase, SmY. The longest homologue, CT6O.10, exhibits a different sequence of smectic phases below the nematic phase: an uniaxial SmA phase, a biaxial SmA_b phase, a tilted SmC phase, and the soft crystalline SmY phase. Interestingly, while in all smectic phases of homologues m = 1–9 the structure is intercalated, with smectic layer thickness $d \sim l/2$, in homologue m = 10 only the SmC has an intercalated structure of molecules; all other smectic phases show interdigitated molecular packing arrangement, with periodicity $d \sim 2l$. The change in structure of the phases between short and long homologues is induced by the competing tendencies toward intercalation, promoted by strong interaction between the mesogenic cores and leading to a structure with layers formed by half the molecule, and bilayer organization promoted by the self-segregation of cyano and alkyl terminal groups. In the case of homologues with m = 8 and m = 9, the frustration in molecular packing is relieved in the SmC phase by the formation of a 2D modulated structure. Interestingly, the strong biaxiality of the SmC phase results in an unusual switching mode detected under the application of an electric field, in which by coupling the dielectric anisotropy with the electric field, molecules in HG cells reorient to give an optical texture without tilt domains, and the switching is accompanied by a considerable increase in the measured birefringence.

Conflicts of interest

There are no conflicts to declare.

Acknowledgements

EG and DP acknowledge the support of the National Science Centre (Poland): (Grant Number 2016/22/A/ST5/00319). RW gratefully acknowledges The Carnegie Trust for the Universities of Scotland for funding the award of a PhD scholarship 2015–2018.

References

1 R. B. Meyer, *Les Houches Summer Sch. Theor. Physics, Mol. Fluids*, Gordon And Breach, New York, 1976, pp. 316–320.
2 I. Dozov, *Europhys. Lett.*, 2001, **56**, 247–253.
3 M. Cestari, S. Diez-Berart, D. A. Dunmur, A. Ferrarini, M. R. De La Fuente, D. J. B. Jackson, D. O. Lopez, G. R. Luckhurst, M. A. Perez-Jubindo, R. M. Richardson, J. Salud, B. A. Timimi and H. Zimmermann, *Phys. Rev. E: Stat., Nonlinear, Soft Matter Phys.*, 2011, **84**, 031704.
4 D. Chen, J. H. Porada, J. B. Hooper, A. Klittnick, Y. Shen, M. R. Tuchband, E. Korbloèa, D. Bedrov, D. M. Walba,

M. A. Glaser, J. E. Maclennan and N. A. Clark, *Proc. Natl. Acad. Sci. U. S. A.*, 2013, **110**, 15931–15936.
5 V. Borshch, Y. K. Kim, J. Xiang, M. Gao, A. Jákli, V. P. Panov, J. K. Vij, C. T. Imrie, M. G. Tamba, G. H. Mehl and O. D. Lavrentovich, *Nat. Commun.*, 2013, **4**, 2635.
6 C. Zhu, M. R. Tuchband, A. Young, M. Shuai, A. Scarbrough, D. M. Walba, J. E. Maclennan, C. Wang, A. Hexemer and N. A. Clark, *Phys. Rev. Lett.*, 2016, 116, DOI: 10.1103/PhysRevLett.116.147803.
7 R. Walker, J. M. D. Storey, C. T. Imrie, D. Pociecha and E. Gorecka, *Chem. – Eur. J.*, 2019, **25**, 13329–13335.
8 C. Greco, G. R. Luckhurst and A. Ferrarini, *Phys. Chem. Chem. Phys.*, 2013, **15**, 14961–14965.
9 A. A. Dawood, M. C. Grossel, G. R. Luckhurst, R. M. Richardson, B. A. Timimi, N. J. Wells and Y. Z. Yousif, *Liq. Cryst.*, 2017, **44**, 106–126.
10 R. J. Mandle, *Soft Matter*, 2016, **12**, 7883–7901.
11 R. J. Mandle and J. W. Goodby, *CrystEngComm*, 2016, **18**, 8794–8802.
12 E. E. Pocock, R. J. Mandle and J. W. Goodby, *Molecules*, 2021, **26**, 532.
13 M. Šepelj, A. Lesac, U. Baumeister, S. Diele, H. L. Nguyen and D. W. Bruce, *J. Mater. Chem.*, 2007, **17**, 1154–1165.
14 D. A. Paterson, C. A. Crawford, D. Pociecha, R. Walker, J. M. D. Storey, E. Gorecka and C. T. Imrie, *Liq. Cryst.*, 2018, **45**, 2341–2351.
15 R. Walker, D. Pociecha, A. Martinez-felipe, J. Storey, E. Gorecka and C. T. Imrie, *Crystals*, 2020, **10**, 175.
16 J. P. Abberley, R. Killah, R. Walker, J. M. D. Storey, C. T. Imrie, M. Salamończyk, C. Zhu, E. Gorecka and D. Pociecha, *Nat. Commun.*, 2018, **9**, 228.
17 M. Salamończyk, N. Vaupotič, D. Pociecha, R. Walker, J. M. D. Storey, C. T. Imrie, C. Wang, C. Zhu and E. Gorecka, *Nat. Commun.*, 2019, **10**, 1922.
18 R. Walker, D. Pociecha, G. J. Strachan, J. M. D. Storey, E. Gorecka and C. T. Imrie, *Soft Matter*, 2019, **15**, 3188–3197.
19 S. P. Sreenilayam, Y. P. Panarin, J. K. Vij, V. P. Panov, A. Lehmann, M. Poppe, M. Prehm and C. Tschierske, *Nat. Commun.*, 2016, **7**, 11369.
20 H. Takezoe, E. Gorecka and M. Čepič, *Rev. Mod. Phys.*, 2010, **82**, 897–937.
21 D. A. Paterson, M. Gao, Y. K. Kim, A. Jamali, K. L. Finley, B. Robles-Hernández, S. Diez-Berart, J. Salud, M. R. De La Fuente, B. A. Timimi, H. Zimmermann, C. Greco, A. Ferrarini, J. M. D. Storey, D. O. López, O. D. Lavrentovich, G. R. Luckhurst and C. T. Imrie, *Soft Matter*, 2016, **12**, 6827–6840.
22 D. A. Paterson, J. P. Abberley, W. T. A. Harrison, J. Storey and C. T. Imrie, *Liq. Cryst.*, 2017, **44**, 127–146.
23 E. E. Pocock, R. J. Mandle and J. W. Goodby, *Soft Matter*, 2018, **14**, 2508–2514.
24 R. J. Mandle, M. P. Stevens and J. W. Goodby, *Liq. Cryst.*, 2017, **44**, 2046–2059.
25 R. Walker, M. Majewska, D. Pociecha, A. Makal, J. M. D. Storey, E. Gorecka and C. T. Imrie, *ChemPhysChem*, 2021, **22**, 461–470.
26 R. Pratibha, N. V. Madhusudana and B. K. Sadashiva, *Europhys. Lett.*, 2007, **80**, 46001.
27 Y. Kimoto, A. Nishizawa, Y. Takanishi, A. Yoshizawa and J. Yamamoto, *Phys. Rev. E: Stat., Nonlinear, Soft Matter Phys.*, 2014, **89**, 42503.
28 J. Prost and P. Barois, *J. Chem. Phys.*, 1983, **80**, 65.
29 Y. Shi, G. Nounesis and S. Kumar, *Phys. Rev. E: Stat., Nonlinear, Soft Matter Phys.*, 1996, **54**, 1570–1573.
30 D. Pociecha, N. Vaupotič, E. Gorecka, J. Mieczkowski and K. Gomola, *J. Mater. Chem.*, 2008, **18**, 881–885.
31 G. S. Attard, R. W. Date, C. T. Imrie, G. R. Luckhurst, S. J. Roskilly, J. M. Seddon and L. Taylor, *Liq. Cryst.*, 1994, **16**, 529–581.
32 C. T. Imrie, P. A. Henderson and J. M. Seddon, *J. Mater. Chem.*, 2004, **14**, 2486–2488.
33 C. T. Imrie, *Liq. Cryst.*, 2006, **33**, 1449–1485.